# $^{58}Ni(^{16}O,^{12}C)^{62}Zn$ reaction at 46 and 60 MeV incident energy

G. P. A. Berg, B. Berthier, J. P. Fouan, J. Gastebois, J. P. Le Fèvre, and M.-C. Lemaire
*Département de Physique Nucléaire, Centre d'Etudes Nucléaires de Saclay, BP 2, 91190 Gif-sur-Yvette, France*
(Received 27 February 1978)

Cross section angular distributions for the $^{16}O$ elastic scattering on $^{58}Ni$ at an incident energy of $E_{16_O} = 60$ MeV and the $^{58}Ni$ $(^{16}O,^{12}C)^{62}Zn$ reaction leading to the strongly excited states at 0.0 MeV, 0.95 MeV, and 3.19 MeV at $E_{16_O} = 46$ MeV and 60 MeV have been measured. Six different sets of optical model parameters are able to reproduce equally well the measured cross section angular distribution of the oxygen elastic scattering. The EFR-DWBA analysis of the $(^{16}O,^{12}C)$ results shows that only one set of surface transparent optical model parameters predicts the $(^{16}O,^{12}O)$ angular distributions at $E_{16_O} = 60$ MeV, while no optical potential was able to provide good fits to the 46 MeV data. The position of the maxima of the "bell shaped" angular distributions at 46 MeV are shifted to forward angles compared to the DWBA calculations. Relative spectroscopic factors obtained from comparison of data and calculations will be compared to previous $(^6Li,d)$ results. Using a $Q3D$ magnetic spectrograph an energy spectrum resolution of 60 keV was obtained for the $^{58}Ni(^{16}O^{12}C)^{62}Zn$ reaction and 13 energy levels are identified in the excitation energy range from 3.19 to 6.30 MeV.

NUCLEAR REACTIONS $^{58}Ni(^{16}O, ^{16}O)$, $E_{16_O} = 60$ MeV; $^{58}Ni(^{16}O, ^{12}C)$, $E_{16_O} = 46$ MeV and 60 MeV; measured $\sigma(\theta)$, $\theta_{lab} = 14°-84°$ for $(^{16}O, ^{16}O)$ and $\theta_{lab} = 3°-36°$ for $(^{16}O, ^{12}C)$, $\Delta\theta_{lab} = 1°$; deduced optical model parameters from elastic scattering; EFR-DWBA analysis; identified 13 energy levels in $^{62}Zn$ between $E_x = 3.19$ MeV and 6.30 MeV, resolution 60 keV.

## I. INTRODUCTION

In recent years single and multinucleon transfer reactions induced by heavy ions have been studied extensively experimentally as well as theoretically. The particular features of these reactions have been summarized in many review articles.[1-6] One of the most interesting aspects of studying multinucleon transfer reactions is to obtain information on four nucleon correlations in nuclei.

The first systematic studies of $2p$-$2n$ transfer reactions on $1f$-$2p$ shell target nuclei were performed with $(^{16}O,^{12}C)$ reaction.[7,8] It has been suggested that the observed strong selectivity in the population of the final states might reveal a quartet structure of nuclei as proposed by Danos and Gillet.[9] However, no reliable nuclear structure information could be obtained because not enough was known about the reaction mechanism. The poor energy resolution of 250 keV in $(^{16}O,^{12}C)$ spectra with silicon detectors has been improved to 60–100 keV for thin targets since quadrupole-dipole-dipole-dipole (Q3D) magnetic spectrographs are used to detect heavy reaction products.[10,11] In the present work the Saclay Q3D spectrograph was used to measure high resolution energy spectra (full width at half maximum ~60 keV) and angular distributions of individual levels in $^{62}Zn$ populated by the $^{58}Ni(^{16}O, ^{12}C)^{62}Zn$ reaction at 46 and 60 MeV incident energies.

Despite several studies the mechanism of the $(^{16}O,^{12}C)$ reaction is not yet well understood. The EFR-DWBA (distorted-wave Born-approximation) calculations which reproduce the $(^{16}O,^{12}C)$ data are often based on optical model (OM) parameters which do not describe the elastic scattering data.[5,12-15] This may be due to the fact that elastic scattering and transfer reactions are sensitive to different regions of the OM potential.[16-18] It has been shown[16] that the elastic scattering is sensitive only to the tail of the OM potential far outside of the nucleus while transfer reactions take place near the nuclear surface. Several studies[19-22] of heavy ion induced one and two particle transfer reactions show that adequate fits to the transfer data can be obtained only with surface transparent potentials. Owing to well known OM ambiguities,[23,24] however, very different types of OM potentials (surface transparent, surface absorption, and weak absorption) can provide equally good fits to elastic scattering data.

We measured the $^{16}O + ^{58}Ni$ elastic scattering angular distributions up to $\theta_{c.m.} = 100°$ at $E_{16_O} = 60$ MeV in order to determine OM parameters necessary for the EFR-DWBA calculations. By refitting existing elastic scattering data[25] OM potentials for 46 MeV incident energy were obtained. The influence of different types of OM parameters on the results of the EFR-DWBA calculations for the measured $^{58}Ni(^{16}O,^{12}C)^{62}Zn$ transitions will be

 

discussed.

It has been shown recently that the failure of EFR-DWBA calculations in reproducing the transfer data may be due to shell model state polarization,[26] neglected in usual DWBA calculations. This effect is expected to be strong for incident energies close to the Coulomb barrier and should decrease with increasing energies. Our analysis of the transfer data taken at 46 and 60 MeV incident energies will be a test of this model.

The question whether the four nucleons transferred in the ($^{16}$O,$^{12}$C) reaction behave like an $\alpha$ particle has been the subject of many discussions.[27-32] Shell model calculations of Kurath and Towner[33] showed that at the nuclear surface the contribution of 0$s$ relative motion dominates over the other components (0$p$, 1$s$, 0$d$, 1$p$, 2$s$). To verify this hypothesis, a quantitative comparison of the relative spectroscopic factors with those derived from the ($^{6}$Li,$d$) reaction,[34] assumed to be a good "$\alpha$ transfer reaction", has been done.

## II. EXPERIMENTAL DETAILS

To investigate the $^{58}$Ni($^{16}$O,$^{16}$O) elastic scattering and the $^{58}$Ni($^{16}$O,$^{12}$C)$^{62}$Zn reaction we used the $^{16}$O beam of 6$^{+}$ atomic charge state from the Saclay super-FN tandem accelerator. The beam was steered into a scattering chamber and focused through a 1.5 × 2.0 mm$^2$ entrance slit on the $^{58}$Ni target which was fixed at 90° to the beam direction. All angular distributions have been measured with a target consisting of a 188 $\mu$g/cm$^2$ thick layer of $^{58}$Ni evaporated on a 30 $\mu$g/cm$^2$ thick carbon foil. The typical resolution for this target was about 150 keV. For the spectra at higher excitation energy a resolution of about 60 keV was obtained with a 30 $\mu$g/cm$^2$ $^{58}$Ni layer on a 10 $\mu$g /cm$^2$ carbon backing. Some examples of $^{12}$C spectra are shown in Fig. 1. The isotopic enrichment of $^{58}$Ni was (99.95 ± 0.01)%. Outgoing reaction products were momentum analyzed in the Saclay Q3D magnetic spectrograph and detected by a 85 cm long gas counter[35] in the focal plane. This counter was a two stage proportional counter filled with a gas mixture of argon-methane (90–10%). The 1 cm thick resistive wire transmission detector delivered the energy loss $\Delta E$ and the position along the focal plane. The 10 cm thick rear detector measured the remaining energy $E_r$. The gas pressure was adjusted to 540 Torr to stop the $^{12}$C ions. Incident ions were particle identified by appropriate limits in the $\Delta E$ and $E_r$ spectra. Some examples of $^{12}$C position spectra are shown in Fig. 1. The solid angle was defined by the Q3D entrance slits. For the measurements at 60 MeV incident energy a relatively small angular acceptance of $\Delta\theta = \pm 5$ mrad was chosen in order to resolve the oscillatory structure of the angular distributions. The azimuthal opening was $\Delta\phi = \pm 40$ mrad for scattering angles $\theta_{lab} < 10°$ and was reduced to $\Delta\phi = \pm 20$ mrad for $\theta_{lab} \leq 10°$ to avoid appreciable deviations of $\theta$ for angles out of the reaction plane. At $E_{^{16}O} = 46$ MeV the angular distributions are structureless and therefore a large

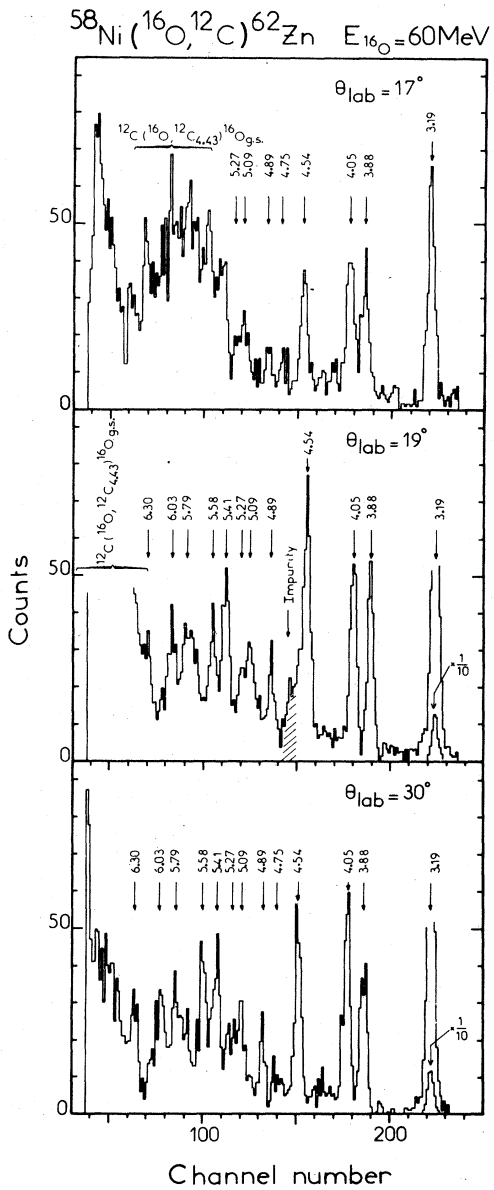


FIG. 1. Sample spectra of the reaction $^{58}$Ni($^{16}$O, $^{12}$C) $^{62}$Zn at three scattering angles $\theta_{lab} = 17°$, 19°, and 30° with identified energy levels between $E_x = 3.19$ and 6.30 MeV. The unknown impurity marked in the 19° spectrum falls in the 17° spectrum right on the doublet at 3.88 and 4.05 MeV. For detailed discussion see Sec. III.

TABLE I. Measured atomic charge state contribution for $^{12}C$ and $^{16}O$ ions.

| Ion | $E_{lab}$ (MeV) | $5^+$ (%) | $6^+$ (%) | $7^+$ (%) | $8^+$ (%) |
|---|---|---|---|---|---|
| $^{12}C$ | 49.04 | 13.5 ± 0.5 | 86.6 ± 3.5 | ... | ... |
| $^{12}C$ | 55.80 | 9.9 ± 0.4 | 90.1 ± 3.6 | ... | ... |
| $^{16}O$ | 54.25 | 0 | 3.17 ± 0.11 | 30.2 ± 1.1 | 66.6 ± 2.4 |
| $^{16}O$ | 56.96 | 0 | 2.70 ± 0.08 | 28.4 ± 0.9 | 68.9 ± 2.1 |

angle opening of $\Delta\theta = \pm 30$ mrad was chosen. The azimuthal angle opening was $\Delta\phi = \pm 35$ mrad for these measurements. In order to monitor the dead time of the analog-to-digital converters (ADC) the total number of events arriving at the ADC and the number of events leaving them were counted in scalers. The ratio of these two scaler counts determined the dead-time correction factor which was typically 2% but always smaller than 6%. All data are properly corrected for these losses. During the experiment the magnetic field of the spectrograph was adjusted to count the most abundant atomic charge state which was the $6^+$ state for the $^{12}C$ ions and the $8^+$ state for the $^{16}O$ ions. We measured the charge state contributions using the ($^{16}O$,$^{12}C$) reaction and the elastic scattering on $^{12}C$ by simply turning around the $^{58}Ni + ^{12}C$ target so that the $^{12}C$ side was facing the incident beam. This allows the outgoing $^{12}C$ and $^{16}O$ ions to obtain equilibrium charge distribution when passing through the $^{58}Ni$ layer. The use of a $^{12}C$ target has the advantages of a large $^{12}C(^{16}O,^{12}C)$ cross section and an easy access to a wide range of ion energies simply by changing the scattering angle $\theta$. In this arrangement the above specified thick target was used for $^{12}C$ while for the $^{16}O$ charge distributions a target of a 30 $\mu g/cm^2$ $^{12}C$ foil with a layer of 80 $\mu g/cm^2$ $^{58}Ni$ was used. Our results shown in Table I are in good agreement with the measurement of Weber *et al.*[36] Charge states smaller than $5^+$ for $^{12}C$ and $6^+$ for $^{16}O$ are assumed to be negligibly small.[37] All data are corrected for charge state losses and correction factors for energies different from the measured ones are calculated by linear interpolation.

A surface barrier detector at $\theta_{lab} = 30°$ was used to monitor elastic scattering from the target. Relative cross sections were obtained by normalizing to the number of counts in the elastic peak of the monitor detector for a particular measurement. In order to determine the normalization factor for the absolute cross section we assumed the elastic scattering of $^{16}O$ on $^{58}Ni$ to be pure Rutherford scattering between $\theta_{lab} = 20°$ and 25°. All cross sections are normalized to the calculated Rutherford cross section in this range of scattering angles. The overall uncertainty of the absolute cross section is estimated to be 10% for the $^{58}Ni(^{16}O,^{12}C)$ reaction. This uncertainty results from the uncertainties in atomic charge state and dead-time correction factor, the error in the ratio of solid angles, and the deviation of the measured elastic scattering from the calculated Rutherford cross section.

## III. EXPERIMENTAL RESULTS

The overall energy resolution in the $^{12}C$ spectra results mainly from the energy spread in the target and the stability of the oxygen beam energy. The resolution of 60 keV obtained with the thin $^{58}Ni$ target allowed to identify 13 energy levels in $^{62}Zn$ between 3.19 and 6.30 MeV using the $^{58}Ni(^{16}O,^{12}C)$ $^{62}Zn$ reaction at 60 MeV incident energy. These energy levels are listed in Table II and compared to results from the ($^6Li$,$d$) work of Fulbright *et al.*[34] Measurements for higher excitation energies $E_x = 6$–10 MeV show many overlapping peaks but no level is dominantly populated.

TABLE II. Identified energy levels in $^{62}Zn$.

| $E_x$ [a] | $E_x$ [b] | $J^\pi$ [c] |
|---|---|---|
| 3.19 ± 0.02 | 3.19 | $3^-$ |
| 3.88 ± 0.03 | 3.84 | $1^-$ |
| 4.05 ± 0.03 | 3.99 | $0^+$ [d] |
| 4.54 ± 0.04 | 4.49 | $(6^+)$ |
| 4.75 ± 0.04 | ... | |
| 4.89 ± 0.04 | 4.96 | |
| 5.09 ± 0.07 | 5.09 | $(1^-)$ |
| 5.27 ± 0.07 | 5.33 | |
| 5.41 ± 0.03 | 5.47 | |
| 5.58 ± 0.04 | | |
| 5.79 ± 0.03 | | |
| 6.03 ± 0.03 | | |
| 6.30 ± 0.03 | | |

[a] This work.
[b] From ($^6Li$,$d$) work of Ref. 34.
[c] Ref. 34 and references therein.
[d] The $0^+$ spin assignment of the state at $E_x = 3.99$ MeV is based on Refs. 43–45 in Ref. 34.

To identify energy levels we measured several spectra for different scattering angles between $\theta = 16°$ and 40°. Three sample spectra are shown in Fig. 1. Energy levels were adopted only if their peaks could be seen at least in three different spectra. In this way impurity peaks can be identified by their different kinematical behavior from the peaks of the $^{62}$Zn levels. A good resolution in the Q3D spectra depends on the appropriate kinematic correction by a magnetic multipole field. Because this correction was set for the best resolution for the $^{58}$Ni($^{16}$O, $^{12}$C)$^{62}$Zn reaction, impurity peaks are usually rather wide as for example the $^{12}$C($^{16}$O, $^{12}$C$^{*}_{4.43\ MeV}$)$^{16}$O$_{g.s.}$ impurity peak on Fig. 1.

The energies of the $^{62}$Zn levels given in Table II are determined using the measured calibration $\rho$ channel, where $\rho$ is the curvature radius of the particle path in the magnetic field $B$. The excitation energy $E_x = 3.19$ MeV of the lowest 3$^-$ state was taken from ($^6$Li,$d$) results of Fulbright *et al.*[34] By changing the magnetic field $B$ the peak of the 3$^-$ state was moved to different counter positions. In first order approximation the calibration $\rho$ channel is linear but shows small deviations from linearity due to the characteristics of the Q3D spectrograph and the counter. Uncertainties of the excitation energies are calculated from the standard deviations of the measurements at different scattering angles. The errors given in Table I include the error of ±20 keV given in Ref. 34 for the 3.19 MeV level.

The selectivity of the ($^{16}$O,$^{12}$C) reaction is similar to the ($^6$Li,$d$) reaction.[34] Strongly excited states are the ground state 0$^+$, the 0.95 MeV 2$^+$ state, the 3.19 MeV 3$^-$ state as well as the levels lying at 3.88, 4.05, and 4.56 MeV excitation energies. On the contrary the 1.80 MeV 2$^+$, the 2.18 MeV 4$^+$, and the 2.74 MeV levels are weakly populated in both reactions. The relative selectivity of the states populated in the ($^{16}$O,$^{12}$C) and the ($^6$Li,$d$) reactions has been discussed by Erskine *et al.*[11] for $^{40}$Ca and by Peng *et al.*[31] for $^{24}$Mg and $^{28}$Si targets.

No evidence was found for the $^{58}$Ni($^{16}$O,$^{12}$C$^{*}_{4.43\ MeV}$) $^{62}$Zn$_{g.s.}$ reaction which should show a Doppler broadened peak at $E_x = 4.43$ MeV. This reaction is of interest because its strong population would indicate that for ($^{16}$O,$^{12}$C) reactions on $^{58}$Ni a two step mechanism via the 4.43 MeV state in $^{12}$C may be important.

The measured cross-section angular distributions of the $^{58}$Ni($^{16}$O,$^{12}$C) $^{62}$Zn reaction leading to the 0$^+$ g.s., 0.95 MeV 2$^+$ state and the 3.19 MeV 3$^-$ state are represented in Fig. 2 and Fig. 3. Numerical results are published elsewhere.[38] The data for 46 MeV incident energy (Fig. 2) are measured for scattering angles $\theta_{c.m.} = 35°$–90° and show typical "bell shape" angular distributions with maxima at about $\theta_{c.m.} = 65°$ for the 0$^+$ and 2$^+$ states and 75° for the 3$^-$ state. Figure 3 shows the data points in the angle range $\theta_{c.m.} = 5°$–45° for $E_{^{16}O} = 60$ MeV. At this energy measurements were taken in 1° steps in the laboratory system in order to resolve the oscillations for the 0$^+$ and 2$^+$ transitions. Missing data points at certain angles

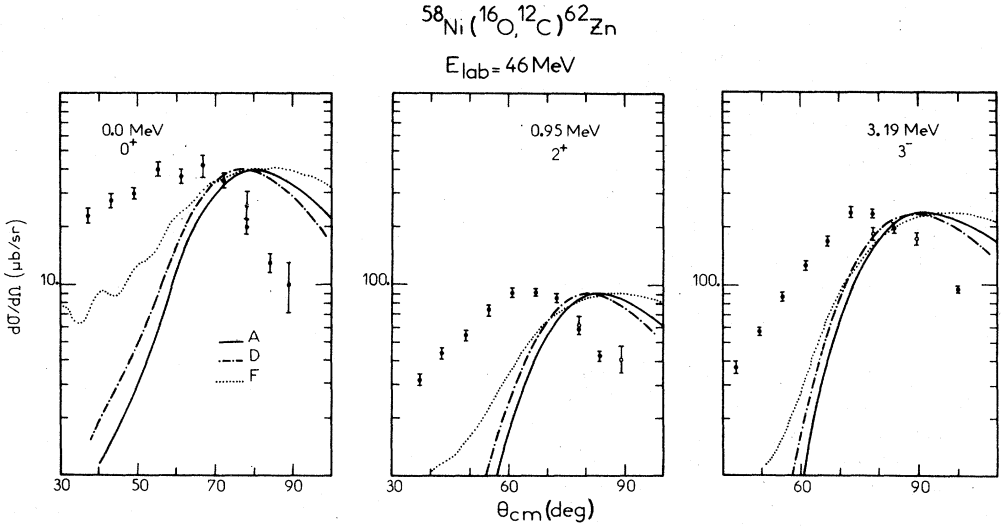


FIG. 2. Measured cross-section angular distributions of the $^{58}$Ni($^{16}$O, $^{12}$C)$^{62}$Zn reaction at 46 MeV incident oxygen energy leading to the strongly excited low lying 0$^+$, 2$^+$, and 3$^-$ states. Error bars indicate statistical errors. The curves A, D, and F represent the EFR-DWBA calculations using the corresponding OM potentials from Table III. Calculations with OM potentials $B$, $C$, and $E$ given in Table III are not shown because they are very similar to curves A and D.

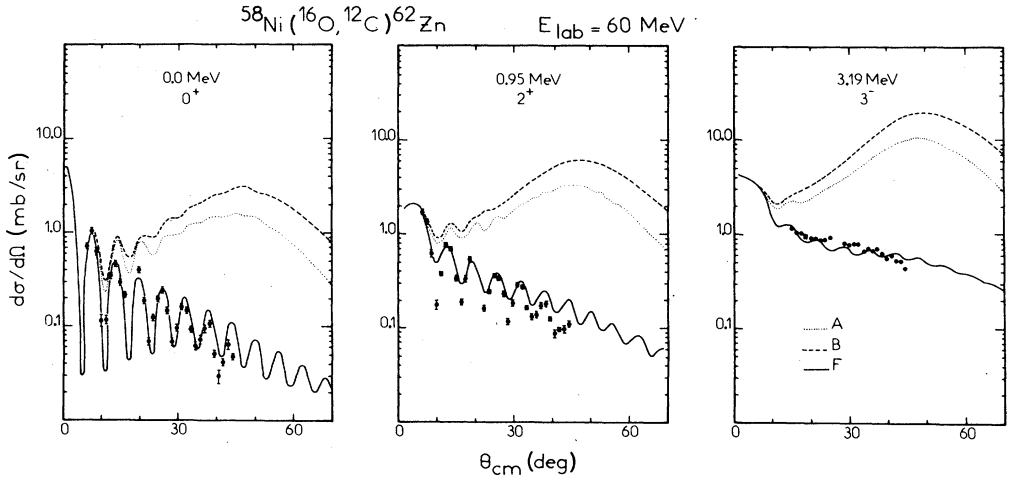


FIG. 3. Measured cross-section angular distributions of the $^{58}$Ni($^{16}$O, $^{12}$C)$^{62}$Zn reaction similar as indicated under Fig. 2 but at 60 MeV incident oxygen energy. Only the EFR-DWBA calculation using OM potential *F* reproduces the experimental data points. Calculations using OM potentials *C*, *D*, and *E* of Table III are not shown but give results very similar to curves A and B.

are due to impurity peaks. The oscillations are most pronounced for the 0$^+$ state. While the oscillations are still present in the 2$^+$ transition they disappear completely in the 3$^-$ transition.

The measurements of angular distributions for the $^{16}$O+$^{58}$Ni elastic scattering in the angular range $\theta_{c.m.} = 18°$–$100°$ are shown in Fig. 4.

## IV. EFR-DWBA ANALYSIS

### A. Elastic scattering and optical model analysis

The analysis of the $^{58}$Ni($^{16}$O,$^{12}$C)$^{62}$Zn data using the exact finite range distorted-wave Born approximation (EFR-DWBA) requires the knowledge of the wave functions which describe the elastic scattering in the entrance and exit channels. To provide the OM parameters necessary to calculate the entrance channel wave function we refitted the $^{16}$O+$^{58}$Ni elastic scattering data at $E_{lab} = 46$ MeV of West *et al.*[25] using six different OM starting parameters from the literature.[25,30,39–41] We employed the OM part of the computer code ECIS[42] using a Woods-Saxon form for the real and imaginary potential. The potential depth, radius, and diffuseness parameters are denoted $V$, $r_v$, $a_v$ and $W$, $r_w$, $a_w$ for the real and the imaginary potentials, respectively. The potential radius is defined as $R = r(A_1^{1/3} + A_2^{1/3})$ for both potentials where $A_1$ and $A_2$ are the mass numbers of projectile and target. All six parameters have been allowed to vary to obtain best fits. The radius parameter of the Coulomb potential $r_c = 1.25$ fm was fixed for all calculations. Table III gives the starting parameters and the fitting results. The OM parameters for $E_{lab} = 60$ MeV shown in the same table are results from fits to our measurements of the $^{16}$O+$^{58}$Ni elastic scattering. Numerical cross sections[38] are published separately. The parameter sets for 46 MeV were used as starting parameters. Figure 4 represents these measurements and the fitting results. The calculations for parameter sets *C* and *E* are not shown, because they are very close to the curves of sets *A* and *B*. All six potentials reproduce the data equally well in the angular range measured from $\theta_{c.m.} = 18°$–$100°$, except for the fact that they fail to reproduce the

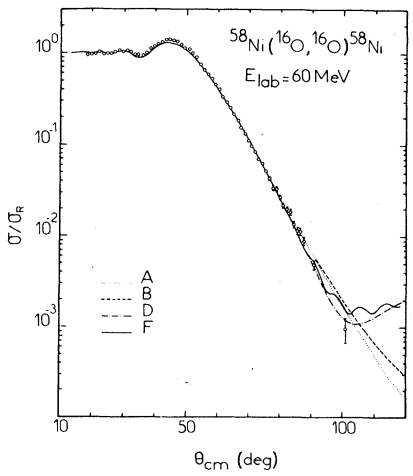


FIG. 4. Measured cross-section angular distributions of the $^{16}$O+$^{58}$Ni elastic scattering at incident energy $E_{^{16}O} = 60$ MeV represented as ratio to the Rutherford cross section $\sigma_R$. The curves A, B, D, F, are calculations using the corresponding OM potentials listed in Table III. For further discussion see Sec. IV A.

TABLE III. Optical model parameters for $^{16}$O + $^{58}$Ni elastic scattering. The Coulomb radius $r_c$ = 1.25 fm for all potentials.

| | | $V$(MeV) | $r_v$ (fm) | $a_v$ (fm) | $W$ (MeV) | $r_w$ (fm) | $a_w$ (fm) | Type of potential [a] | Starting parameters |
|---|---|---|---|---|---|---|---|---|---|
| A | 46 MeV | 85.4 | 1.22 | 0.498 | 39.2 | 1.204 | 0.476 | SA | Ref. 25 |
| | 60 MeV | " | " | " | " | " | " | | |
| B | 46 MeV | 70.0 | 1.202 | 0.57 | 106.6 | 1.202 | .39 | ST | Ref. 39 (ST16) |
| | 60 MeV | 67.7 | 1.196 | 0.574 | 116.8 | 1.195 | .386 | | |
| C | 46 MeV | 21.42 | 1.307 | 0.552 | 7.427 | 1.37 | .448 | WA | Ref. 40 |
| | 60 MeV | 20.97 | 1.313 | 0.554 | 9.677 | 1.357 | .360 | | |
| D | 46 MeV | 74.35 | 1.35 | 0.337 | 78.0 | 1.342 | .174 | ST | Ref. 30 |
| | 60 MeV | 70.15 | 1.343 | 0.339 | 76.39 | 1.344 | .156 | | |
| E | 46 MeV | 31.2 | 1.31 | 0.49 | 42.3 | 1.25 | .43 | ST | Ref. 41 ($^{64}$Ni) |
| | 60 MeV | 29.4 | 1.311 | 0.488 | 36.5 | 1.245 | .421 | | |
| F | 46 MeV | 40.74 | 1.303 | 0.473 | 59.19 | 1.216 | .164 | ST | ... |
| | 60 MeV | 45.09 | 1.298 | 0.461 | 57.39 | 1.217 | .163 | | |

[a] SA = surface absorption, ST = surface transparent, WA = weak absorption.

maximum at the rainbow angle $\theta_{c.m.} \simeq 45°$ by about 10%. For scattering angles $\theta_{c.m.} > 100°$ the calculated cross sections for the sets $A$, $B$, $C$, and $E$ continue to drop while the curves for $D$ and $F$ remain nearly constant with a value of $\sigma/\sigma_R \simeq 10^{-3}$. A typical feature of the parameter sets $D$ and $F$ is the relatively small imaginary diffuseness of $a_w \sim 0.16$ compared to $a_w \gtrsim 0.37$ for all other potentials. This small value of $a_w$ produces a strong surface transparency of the potentials $D$ and $F$ which seems to be necessary to provide the oscillatory structure of the EFR-DWBA calculations.

### B. Description of EFR-DWBA calculations

In order to analyze the measured $^{58}$Ni($^{16}$O,$^{12}$C) $^{62}$Zn angular distributions, which have been presented in Sec. III, we performed calculations in the exact finite range distorted-wave Born approximation (EFR-DWBA) employing the computer code SATURN-MARS-1.[43,44] The two proton–two neutron transfer was treated in the cluster approximation and the transferred particles were considered to be an $\alpha$ cluster in its 0$s$ ground state. Since only one internal state of the $\alpha$ cluster and a single value of the principal quantum number $N$ for the description of the center of mass motion of the $\alpha$ cluster are assumed, the experimental cross section can be written as

$$\sigma_{exp} = R \cdot C_1^2 S_1 \cdot C_2^2 S_2 \cdot \sigma_{DWBA}, \quad (1)$$

where $\sigma_{DWBA}$ is the calculated cross section and $C_1^2 S_1$ and $C_2^2 S_2$ denote the spectroscopic factors for the light system 1 ($^{16}$O-$^{12}$C) and the heavy system 2 ($^{58}$Ni-$^{62}$Zn) with $C_1$ and $C_2$ the usual isospin Clebsch-Gordan coefficients. The renormalization factor $R$ accounts for the discrepancies in magnitude between the calculated and the measured cross sections. It is often referred to as "unhappiness factor." Its origin is not yet clear. For a more detailed discussion see Refs. 15 and 26. Because of this normalization problem, only relative spectroscopic factors can be extracted from comparison of experimental and theoretical cross sections.

Woods-Saxon potentials were used to calculate bound state wave functions. The potential geometry was fixed to $R = 1.25$ fm $A^{1/3}$, where $A$ is the mass number of the $^{12}$C or $^{58}$Ni core, and a diffuseness value of $a = 0.65$ fm. The potential depth was adjusted to reproduce the experimental binding energy of the $\alpha$ cluster in the system core + $\alpha$. The number of nodes $N$ and the orbital angular momentum $L$ for the bound state wave functions are listed in Table IV. Assuming the $\alpha$ cluster to be in an 0$s$ state of the internal motion, energy and parity conservation require the Talmi-Moshin-

TABLE IV. Number of nodes $N$ and angular orbital momenta $L$ used for the bound states.

| | $J^\pi$ | $E_x$ (MeV) | $N$ | $L$ |
|---|---|---|---|---|
| $^{12}$C + $\alpha$ | $0^+$ | 0 | 2 | 0 |
| $^{58}$Ni + $\alpha$ | $0^+$ | 0 | 6 | 0 |
| | $2^+$ | 0.95 | 5 | 2 |
| | $3^-$ | 3.19 | 5 | 3 |

sky[45] relationship:

$$2N+L=\sum_{i=1}^{4}(2n_i+l_i)\,. \tag{2}$$

Here $n_i$ and $l_i$ are the number of nodes and orbital angular momenta of harmonic oscillator states of the $^{12}$C and $^{58}$Ni cores into which the four nucleons go. Owing to incomplete treatment of the residual interaction potential in the post and prior representation, DWBA calculations show different results for these two representations. It has been shown by DeVries[46] that EFR-DWBA calculations of multinucleon transfer reactions using the "post" representation and including the Coulomb interaction terms will reproduce the magnitudes of these reactions with deviations of less than 20%. Therefore the EFR-DWBA computer code SATURN-MARS-1 has been modified to include the Coulomb terms in the interaction potentials[47] and we have used the post representation.

In the code SATURN-MARS-1 optical model parameters are used to calculate the wave functions of the elastic scattering in the entrance and exit channels. The entrance channel potentials were determined by fitting experimental cross-section angular distributions of the $^{16}$O+$^{58}$Ni elastic scattering. This is described in subsection A. Since no OM parameters for the exit channel are available the same potential parameters were used in exit and entrance channel.

### C. Results

Results of EFR-DWBA calculations of cross-section angular distributions for the $^{58}$Ni($^{16}$O,$^{12}$C)$^{62}$Zn reactions leading to the $0^+$ ground state, 0.95 MeV $2^+$ and 3.19 MeV $3^-$ states are shown in Fig. 2 and Fig. 3 together with experimental results already presented in Sec. III. Data and theoretical curves for 46 MeV incident energy (Fig. 2) show typical "bell shape" angular distributions but the positions of all experimental maxima are shifted about 15° to forward angles with respect to the calculated maxima. DWBA calculations for all OM parameters (sets *A*-*F*) listed in Table III were carried out but only curves for *A*,*D*,*F* are shown in Fig. 3 because results for sets *B*, *C*, and *E* are very similar to curves *A* and *D*. For details of the DWBA calculations see Sec. IV B.

It has been shown recently by Delic *et al.*[26] that the use of two-center shell model wave functions in EFR-DWBA calculations can produce a forward shift of the angular distribution maxima of about 20° compared to usual EFR-DWBA calculations. At higher energies polarization effects calculated in the adiabatic limit should diminish and the usual EFR-DWBA should be an adequate description of the transfer reactions.

The experimental and theoretical results for 60 MeV incident energy are shown in Fig. 3. For scattering angles smaller than about $\theta_{c.m.}=8°$ DWBA calculations for all OM potentials *A*–*F* give the same shape but only potential *F* provides good representation of the data at $\theta_{c.m.}>8°$. The potentials *A*–*E* produce "bell shape" angular distributions. In Fig. 3 only results of the calculations with OM potentials *A* and *B* are shown because *C* and *E* give similar results.

The data points of the $0^+$ ground state are in excellent agreement with the calculations using potential *F* in the measured angular range except for small deviations near $\theta_{c.m.}=40°$. The calculation shows the large maximum at $\theta_{c.m.}=0°$ typical for $L=0$ transitions. The experimental angular distributions of the 0.95 MeV $2^+$ state ($L=2$) is not as well reproduced by the EFR-DWBA calculations as the $0^+$ ground state using potential *F*. In particular the experimental minima are not as deep as in the calculations. The individual *M* contributions of the $L=2$ transition are displayed in Fig. 5. It can be seen that a small misrepresentation of the magnitudes and phases of the *M* contributions can easily wash out the deep minima without changing very much the maxima. The experimental and theoretical angular distributions of the 3.19 MeV $3^-$ state are displayed in Fig. 3. For this $L=3$ transition the oscillations are almost completely washed out. This feature, due to the increasing number of contributing magnetic substates (Fig. 5), has already been observed for $L\neq 0$ transitions of the ($^{16}$O,$^{12}$C) reaction on other target nuclei.[31]

The factors $R\cdot C_1^2 S_1\cdot C_2^2 S_2$ containing the spec-

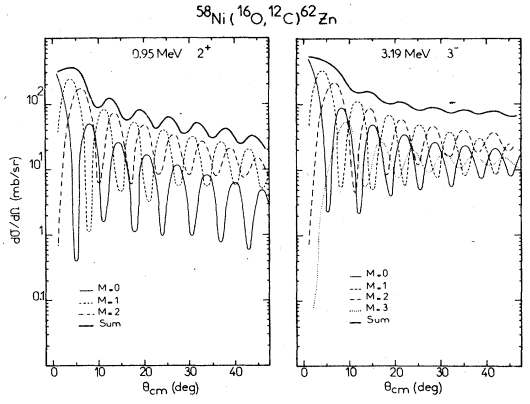


FIG. 5. EFR-DWBA calculations for the 0.95 MeV $2^+$ and 3.19 MeV $3^-$ states identical to the calculations in Fig. 3 are shown (SUM) together with the contributions of different magnetic substates (*M*).

TABLE V. Experimental and theoretical relative spectroscopic factors $C_1^2S_1 \cdot C_2^2S_2/(C_1^2S_1 \cdot C_2^2S_2)_{g.s.}$.

| | | Experimental | | | | | |
|---|---|---|---|---|---|---|---|
| | | ($^{16}$O,$^{12}$C) [a] | | ($^6$Li,$d$) [b] | | ($^{12}$C$^8$Be) [c] | Theoretical ($^{16}$O,$^{12}$C) [d] |
| $E$ (MeV) | $J^\pi, L$ | 46 MeV | 60 MeV | SBF | III | | Shell model |
| 0.0 | $0^+$ 0 | 1(1.9) [e] | 1(4.3) | 1(0.20) | 1(0.15) | 1 | 1($3.10^{-3}$) |
| 0.95 | $2^+$ 2 | 0.42 | 0.40 | 0.36 | 0.29 | 0.35 | 0.55 |
| 3.19 | $3^-$ 3 | 0.38 | 0.55 | 0.39 | 0.37 | ••• | ••• |

[a] This work.
[b] Ref. 34.
[c] Ref. 48.
[d] Shell model calculations of $C_1^2S_1$ (system: $^{16}$O–$^{12}$C) in Ref. 49 and $C_2^2S_2$ (system: $^{58}$Ni–$^{62}$Zn) in Ref. 50. The relative spectroscopic factors are independent of the type of the $\alpha$-stripping reaction.
[e] Absolute spectroscopic factors $R \cdot C_1^2S_1 \cdot C_2^2S_2$ in parentheses.

troscopic factors have been determined according to formula (1) by comparing experimental and theoretical cross sections calculated with OM potential $F$. In Table V the spectroscopic factors relative to the ground state $C_1^2S_1 \cdot C_2^2S_2 / (C_1^2S_1 \cdot C_2^2S_2)_{g.s.}$ are listed for a better comparison with results of the ($^6$Li,$d$) reaction[34] and the ($^{12}$C,$^8$Be) reaction.[48] Theoretical spectroscopic factors for the $0^+$ and the $2^+$ states shown in Table V are obtained from shell model calculations of $C^2S$. [See Bennett *et al.*[49] for the ($^{58}$Ni-$^{62}$Zn) system and Kurath *et al.*[50] for the ($^{16}$O-$^{12}$C) system.]

The experimental relative spectroscopic factors of the 0.95 MeV $2^+$ state for the ($^{16}$O,$^{12}$C) reaction are 0.42 and 0.40 at 46 and 60 MeV. This is 10–15% larger compared to the results from ($^6$Li,$d$) and ($^{12}$C,$^8$Be) reactions. Our result for the 3.19 MeV $3^-$ state at 46 MeV is $C_1^2S_1 \cdot C_2^2S_2 / (C_1^2S_1 \cdot C_2^2S_2)_{g.s.} = 0.38$ which is almost identical to the ($^6$Li,$d$) result. For the 60 MeV data we obtain a value of 0.55 which is about 40% larger than the results at 46 MeV. This gives the contradictory result that the 60 MeV data are better reproduced by the DWBA while the spectroscopic factors for 46 MeV agree better with the ($^6$Li,$d$) results.

In order to estimate the sensitivity of spectroscopic factors on the bound state wave function we changed the radius of the real Woods-Saxon potential in which the form factor is calculated from 1.25 to 1.35 fm. This increases the EFR-DWBA cross sections by a factor of 3.2 for all levels and therefore does not change the relative spectroscopic factors.

## V. SUMMARY

In this work the $^{58}$Ni($^{16}$O,$^{12}$C)$^{62}$Zn reaction has been investigated. We measured cross-section angular distributions at 46 and 60 MeV incident energies and EFR-DWBA calculations have been carried out. From this investigation we draw the following conclusions:

(1) The relative selectivity of ($^{16}$O,$^{12}$C) and ($^6$Li,$d$) reactions on $^{58}$Ni is very similar.

(2) No evidence was found for the $^{58}$Ni($^{16}$O,$^{12}$C$^*_{4.43\ MeV}$)$^{62}$Zn$_{g.s.}$ reaction.

(3) $^{58}$Ni($^{16}$O,$^{12}$C)$^{62}$Zn angular distributions are "bell shaped" at 46 MeV and no $L$ dependence was found. On the contrary the angular distributions at 60 MeV show strong oscillations which are different for $L=0$ and $L=2$ transitions. No oscillations are found in the measured $L=3$ transition which is due to the incoherent sum over contributions from several magnetic substates.

(4) Using the surface transparent OM potential $F$, exact finite range DWBA calculations reproduce fairly well the 60 MeV transfer data. Simultaneously potential $F$ provides good fits to the measured $^{16}$O+$^{58}$Ni elastic scattering data. No DWBA calculation was able to reproduce the 46 MeV transfer data. The experimental maxima of the "bell shape" angular distributions are shifted about 15° to forward angles compared to all calculations.

(5) The improving agreement observed between EFR-DWBA calculations and the experimental data with increasing energy qualitatively supports the idea proposed by Delic *et al.*[31] that shell model state polarizations have to be taken into account for large collision times.

(6) Relative spectroscopic factors between different "$\alpha$-transfer" reactions and calculations agree within about ±20%. These deviations can be attributed to sensitivities of spectroscopic factors to variations in the form factors and the optical model parameters used in the EFR-DWBA calculations.

[1]M.-C. Lemaire, Phys. Rep. 7C, 281 (1973).
[2]W. von Oertzen, *Nuclear Spectroscopy and Reactions*, edited by J. Cerny (Academic, New York, 1974), part B.
[3]K. S. Low, J. Phys. (Paris) Suppl. 37, C5-15 (1976).
[4]S. Kahana and A. J. Baltz, Adv. Nucl. Phys. 9, 1 (1977).
[5]D. G. Kovar, in *Proceedings of the International Conference on Reactions between Complex Nuclei, Nashville, Tennessee, 1974*, edited by R. L. Robinson, F. K. McGowan, J. B. Ball, and J. H. Hamilton (North-Holland, Amsterdam, 1974), Vol. 2, p. 235.
[6]A. J. Baltz, Symposium on macroscopic features on heavy ion collisions, Argonne, Illinois (unpublished), Vol. 1, p. 65.
[7]H. Faraggi, M.-C. Lemaire, J.-M. Loiseaux, M. C. Mermaz, and A. Papineau, Phys. Rev. C 4, 1375 (1971).
[8]H. Faraggi, A. Jaffrin, M.-C. Lemaire, M. C. Mermaz, J.-C. Faivre, J. Gastebois, B. G. Harvey, J.-M. Loiseaux, and A. Papineau, Ann. Phys. (N.Y.) 66, 905 (1971).
[9]M. Danos and V. Gillet, Phys. Rev. 161, 1034 (1967).
[10]L. Bianchi, E. Cotton, and A. Papineau, Proceedings of the European Conference on Nuclear Physics, Aix-en-Provence, 1972 [J. Phys. (Paris) Suppl. 2, 82 (1972)].
[11]J. R. Erskine, W. Henning, and L. R. Greenwood, Phys. Lett. 47B, 335 (1973).
[12]H. J. Koerner, G. C. Morrison, L. R. Greenwood, and R. H. Siemssen, Phys. Rev. C 7, 107 (1973).
[13]J. L. C. Ford, Jr., K. S. Toth, G. R. Satchler, D. C. Hensley, L. W. Owen, R. M. DeVries, R. M. Gaedke, P. J. Riley, and S. T. Thornton, Phys. Rev. C 10, 1429 (1974).
[14]W. Henning, D. G. Kovar, J. R. Erskine, and L. R. Greenwood, Phys. Lett. 55B, 49 (1975).
[15]Y. Eisen, H. T. Fortune, W. Henning, D. G. Kovar, S. Vigdor, and B. Zeidman, Phys. Rev. C 13, 699 (1976).
[16]G. R. Satchler, Nucl. Phys. A279, 493 (1977).
[17]P. J. Moffa, C. B. Dover, and J. P. Vary, Phys. Rev. C 13, 147 (1976).
[18]O. Hansen and J. D. Garrett, J. Phys. (Paris) Suppl. 37, C5-1 (1976).
[19]M.-C. Lemaire, M. C. Mermaz, H. Sztark, and A. Cunsolo, Phys. Rev. C 10, 1103 (1974).
[20]E. H. Auerbach, A. J. Baltz, P. D. Bond, C. Chasman, J. D. Garrett, K. W. Jones, S. Kahana, M. J. Levine, M. Schneider, A. Z. Schwarzchild, and G. E. Thorn, Phys. Rev. Lett. 30, 1078 (1973).
[21]M. J. Levine, A. J. Baltz, P. D. Bond, J. D. Garrett, S. Kahana, and G. E. Thorn, Phys. Rev. C 10, 1602 (1974).
[22]A. J. Baltz, P. D. Bond, J. D. Garrett, and S. Kahana, Phys. Rev. C 12, 136 (1975).
[23]R. Satchler, Symposium on macroscopic features on heavy ion collisions, Argonne, Illinois, 1976 (unpublished), Vol. 1, p. 33.
[24]D. M. Brink, J. Phys. (Paris) Suppl. 37, C5-47 (1976).
[25]L. West, Jr., K. W. Kemper, and N. R. Fletcher, Phys. Rev. C 11, 859 (1975).
[26]G. Delic, K. Pruess, L. A. Charlton, and N. K. Glendenning, Phys. Lett. 69B, 20 (1977).
[27]J. V. Maher, K. A. Erb, G. H. Wedberg, J. L. Ricci, and R. W. Miller, Phys. Rev. Lett. 29, 291 (1972).
[28]L. A. Charlton and D. Robson, Phys. Rev. Lett. 32, 946 (1974).
[29]M. F. Werby and W. Tobocman, Phys. Rev. C 10, 1022 (1974).
[30]J. R. Erskine, W. Henning, D. G. Kovar, L. R. Greenwood, and R. M. DeVries, Phys. Rev. Lett. 34, 680 (1975).
[31]J. C. Peng, J. V. Maher, W. Oelert, D. A. Sink, C. M. Cheng, and H. S. Song, Nucl. Phys. A264, 312 (1976).
[32]R. M. DeVries, Phys. Rev. Lett. 30, 666 (1973).
[33]D. Kurath and I. Towner, Nucl. Phys. 222, 1 (1974).
[34]H. W. Fulbright, C. L. Bennett, R. A. Lindgren, R. G. Markham, S. C. Mc Guire, G. C. Morrison, U. Strohbusch, and J. Toke, Nucl. Phys. A284, 329 (1977).
[35]B. Berthier, E. Chamaux, and J. P. Fouan, Note No. CEA N-1959, 1975–1976 (unpublished), p. 71.
[36]D. J. Weber, N. M. Hintz, and D. Dehnhard, Nucl. Instrum. Methods 124, 317 (1975).
[37]J. B. Marion and F. C. Young, *Nuclear Reaction Analysis* (North-Holland, Amsterdam, 1968).
[38]See AIP document no. PAPS 18-2204-4 pages of numerical results of cross-section angular distributions shown in Figs. 2–4. Order by PAPS number and journal reference from American Institute of Physics, Physics Auxiliary Publication Service, 335 East 45th Street, New York, N.Y. 10017. The price is $1.50 for each microfiche (98 pages), or $5 for photocopies of up to 30 pages with $0.15 for each additional page over 30 pages. Airmail additional. Make checks payable to the American Institute of Physics. This material also appears in *Current Physics Microform*, the monthly microfilm edition of the complete set of journals published by AIP, on the frames immediately following this journal article.
[39]M. S. Zisman, R. M. DeVries, J. G. Cramer, K. L. Liu, Y. D. Chan, and B. Cuengco, Phys. Rev. C 11, 809 (1975).
[40]P. R. Christensen, I. Chernov, E. E. Gross, R. Stokstad, and F. Videback, Nucl. Phys. A207, 433 (1973).
[41]M. E. Cobern, N. Lisbona, and M. C. Mermaz, Phys. Rev. C 13, 674 (1976).
[42]J. Raynal, Coupled channel code ECIS, Saclay Report No. DPh/T/72-48, 1971 (unpublished).
[43]T. Tamura and K. S. Low, Comp. Phys. Comm. 8, 349 (1974).
[44]K. S. Low and T. Tamura, Phys. Rev. C 11, 789 (1975).
[45]T. A. Brody and M. Moshinsky, *Tables of Transformation Brackets for Nuclear Shell Model Calculations* (Gordon and Breach, New York, 1967).
[46]R. M. DeVries, Phys. Rev. C 11, 2105 (1975).
[47]J. P. Le Fèvre, Note No. CEA-N-1959, 1975–1976 (unpublished), p. 36.
[48]E. Mathiak, K. A. Eberhard, J. G. Cramer, H. H. Rossner, J. Stettmeier, and A. Weidinger, Nucl. Phys. A259, 129 (1976).
[49]C. L. Bennett, Nucl. Phys. A284, 301 (1977).
[50]D. Kurath, Phys. Rev. C 7, 1390 (1973).